

## Electronic Supplementary Information

### **ZnFe<sub>2</sub>O<sub>4</sub>@C/graphene nanocomposite as excellent anode materials for lithium batteries**

Li Lin, Qinmin Pan\*

(State Key Laboratory of Robotics and Systems, School of Chemical Engineering and Technology, Harbin

Institute of Technology, Harbin 150001, *P. R.* China)

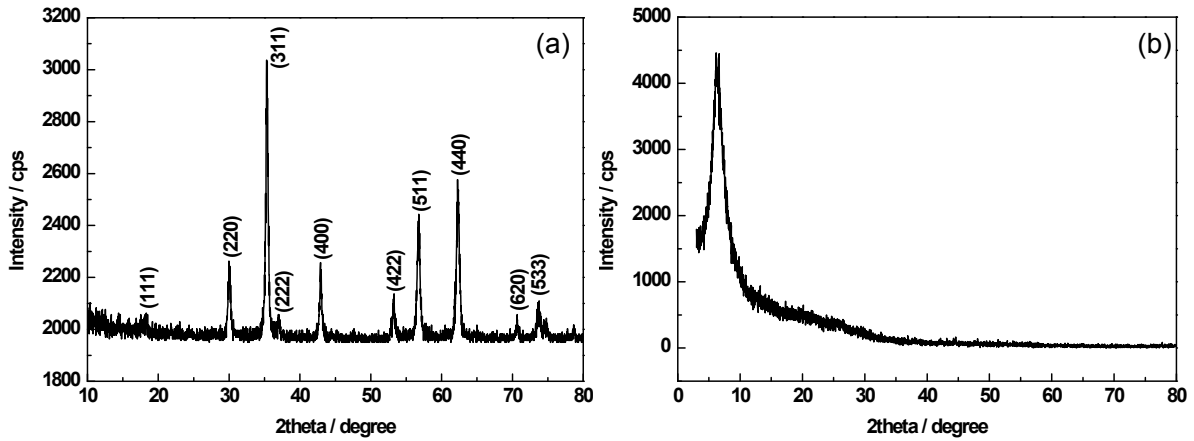


Fig. S1. XRD patterns of (a) ZnFe<sub>2</sub>O<sub>4</sub> nanoparticles and (b) graphite oxide (GO).

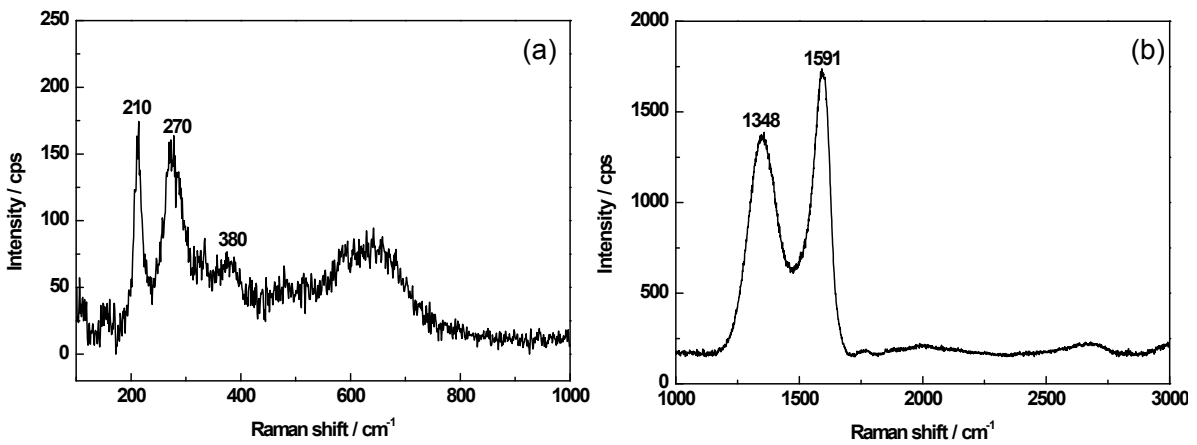


Fig. S2. Raman spectra of (a) ZnFe<sub>2</sub>O<sub>4</sub> nanoparticles and (b) graphite oxide.

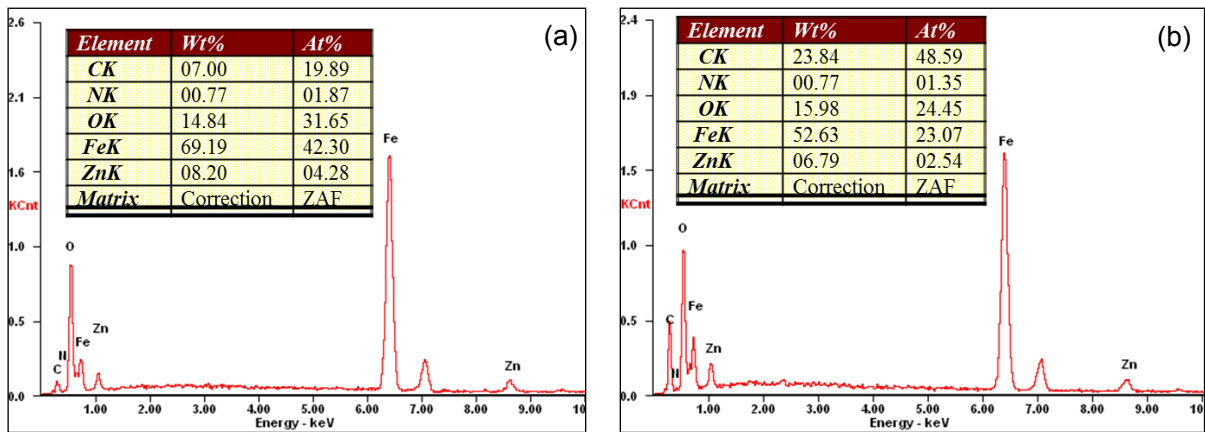


Fig. S3. EDX plots of (a) core-shell ZnFe<sub>2</sub>O<sub>4</sub>@C nanoparticles and (b) ZnFe<sub>2</sub>O<sub>4</sub>@C/G nanocomposite.

Fig. S3 is the EDX plots of ZnFe<sub>2</sub>O<sub>4</sub>@C nanoparticles and ZnFe<sub>2</sub>O<sub>4</sub>@C/G nanocomposite. Both samples show a low Zn/Fe mole ratio. The low Zn content is mainly attributed to the following reasons. Firstly, owing to relatively low content of Zn in ZnFe<sub>2</sub>O<sub>4</sub>@C nanoparticles, the characteristic peaks of Zn may be overlapped by

the continuum X-rays produced in the excitation process. Secondly, X-rays might be absorbed by other atoms of the nanoparticles. Especially, the carbon shells of the nanoparticles may accelerate the absorption.<sup>1</sup> All these factors reduce the detected intensity of Zn element.

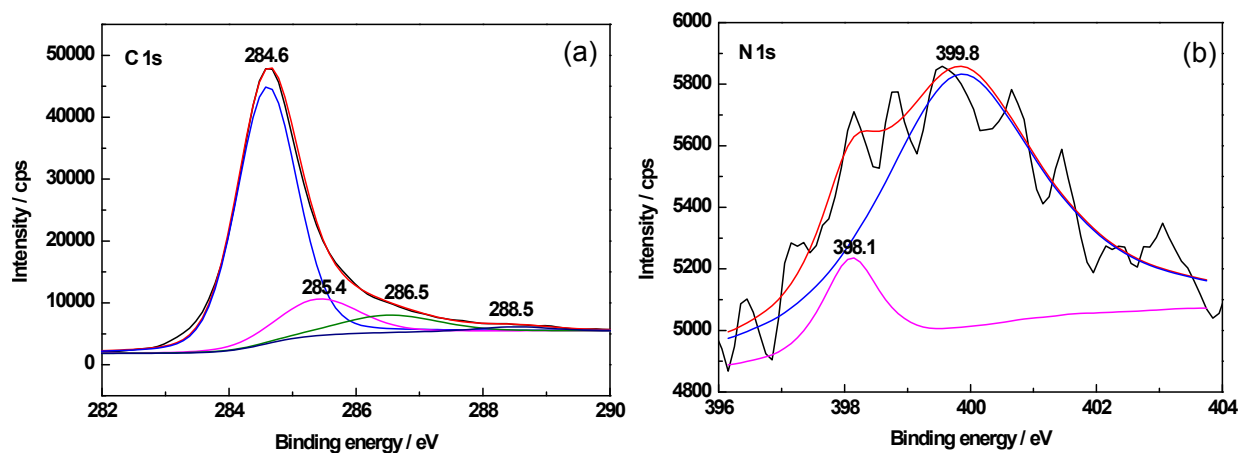
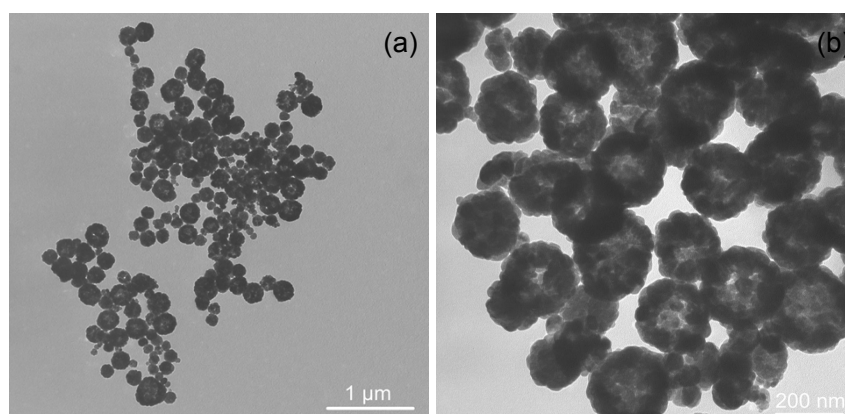


Fig. S4. C 1s (a) and N 1s (b) spectra of ZnFe<sub>2</sub>O<sub>4</sub>@C/G nanocomposite.

XPS measurement was performed to investigate the surface chemistry of ZnFe<sub>2</sub>O<sub>4</sub>@C/G nanocomposite. Four peaks at 284.6 eV, 285.4 eV, 286.5 eV and 288.5 eV are observed in the C 1s spectrum (Fig. S4a), corresponding to the components of C-C, C-N, C=N and C=O, respectively.<sup>2,3</sup> N 1s spectrum (Fig. S4b) shows two components of C-N (399.8 eV) and C=N (398.1 eV), which is consistent with the previous report on N-doped carbon coated Fe<sub>3</sub>O<sub>4</sub> composites.<sup>4</sup>



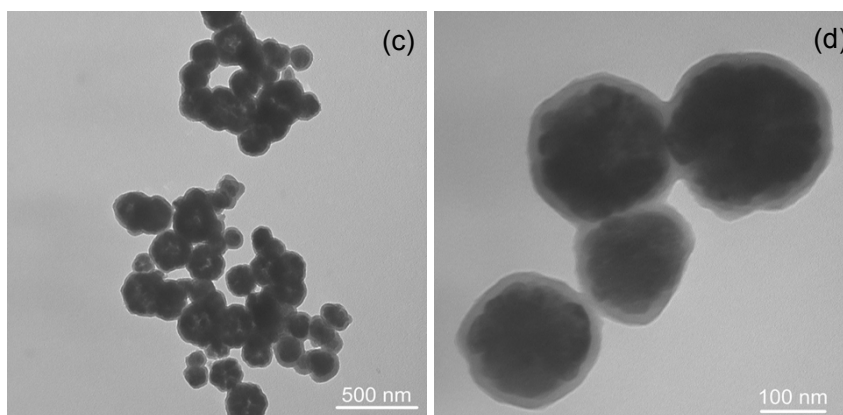


Fig. S5. TEM images of (a, b) ZnFe<sub>2</sub>O<sub>4</sub> nanoparticles and (c, d) core-shell ZnFe<sub>2</sub>O<sub>4</sub>@PDA nanoparticles.

Fig. S5 shows the TEM images of the pristine ZnFe<sub>2</sub>O<sub>4</sub> and core-shell ZnFe<sub>2</sub>O<sub>4</sub>@PDA nanoparticles. The former has a diameter of ~200 nm (Fig. S5a-5b), while the later is uniformly encapsulated by polydopamine (PDA) layers with average thickness of ~20 nm (Fig. S5c-5d). The PDA layers on the nanoparticles are homogenous and continuous, suggesting that polydopamine has high affinity to ZnFe<sub>2</sub>O<sub>4</sub> nanoparticles and thus reducing severe agglomeration to some extent.

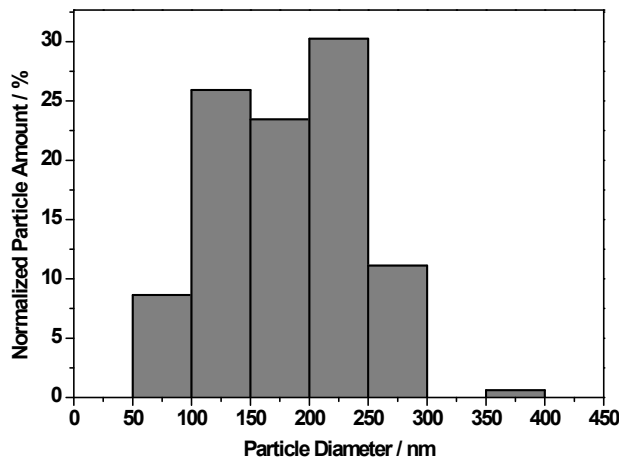


Fig. S6 Size distribution of ZnFe<sub>2</sub>O<sub>4</sub> nanoparticles.

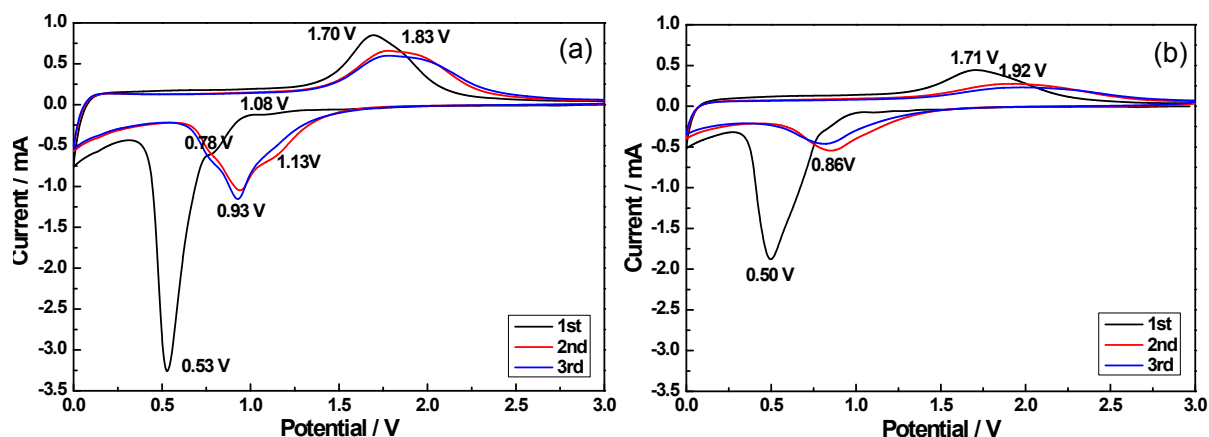


Fig. S7. Cyclic voltammograms of the (a)  $\text{ZnFe}_2\text{O}_4@\text{C}/\text{G}$  and (b)  $\text{ZnFe}_2\text{O}_4@\text{C}$  electrodes.

Fig. S7a shows the CV curves of the  $\text{ZnFe}_2\text{O}_4@\text{C}/\text{G}$  electrode in the first three cycles. In the initial cathodic process, a sharp peak appears at 0.53 V, indicating the conversion of  $\text{ZnFe}_2\text{O}_4$  into  $\text{Zn}^0$ ,  $\text{Fe}^0$ ,  $\text{Li}_2\text{O}$ , as well as the formation of Li-Zn alloy and solid electrolyte interface (SEI) film.<sup>5,6</sup> A small cathodic peak located at 1.08-0.78 V is attributed to the incomplete lithiation of  $\text{ZnFe}_2\text{O}_4$  to  $\text{Li}_{0.2}\text{ZnFe}_2\text{O}_4$  or  $\text{Li}_{0.5}\text{ZnFe}_2\text{O}_4$  and  $\text{Li}_2\text{ZnFe}_2\text{O}_4$ .<sup>5,7</sup> This peak is not observed for the CV curves of the  $\text{ZnFe}_2\text{O}_4@\text{C}$  electrode (Fig. S7b). In the subsequent anodic process, a peak ascribed to the de-alloying of Li-Zn and oxidation of  $\text{Zn}^0$ ,  $\text{Fe}^0$  to  $\text{Zn}^{2+}$ ,  $\text{Fe}^{3+}$  is observed at 1.7 V.<sup>5,8</sup> In the subsequent scanning cycles, both cathodic and anodic peaks shift to 0.93 and 1.83 V with decreased intensity, respectively, suggesting the variation of  $\text{ZnFe}_2\text{O}_4$  structure and the presence of irreversible capacity loss.<sup>5</sup> However, the CV curves of the  $\text{ZnFe}_2\text{O}_4@\text{C}/\text{G}$  electrode show better reproducibility than those of its  $\text{ZnFe}_2\text{O}_4@\text{C}$  counterpart, implying that the presence of graphene is beneficial for the reversibility of  $\text{ZnFe}_2\text{O}_4$ -based electrodes.

## References

1. J. I. Goldstein, D. E. Newbury, P. Echlin, D. C. Joy, C. E. Lyman, E. Lifshin, L. Sawyer and J. R. Michael, Scanning Electron Microscopy and X-Ray Microanalysis [M], Third Edition, New York, Springer, 2003.
2. Q. Zhu and Q. M. Pan, *ACS Nano*, 2014, **8**, 1402–1409.
3. F. T. Liu, F. H. Sun and Q. M. Pan, *J. Mater. Chem. A*, 2014, **2**, 11365–11371.
4. C. Lei, F. Han, D. Li, W. C. Li, Q. Sun, X. Q. Zhang and A. H. Lu, *Nanoscale*, 2013, **5**, 1168–1175.
5. D. Bresser, E. Paillard, R. Kloepsch, S. Krueger, M. Fiedler, R. Schmitz, D. Baither, M. Winter and S. Passerini, *Adv. Energy Mater.*, 2012, **3**, 513–523.
6. Y. Sharma, N. Sharma, G. V. S. Rao and B. V. R. Chowdari, *Electrochim. Acta*, 2008, **53**, 2380–2385.
7. X. Guo, X. Lu, X. Fang, Y. Mao, Z. Wang, L. Chen, X. Xu, H. Yang and Y. Liu, *Electrochem. Commun.*, 2010, **12**, 847–850.
8. J. Sui, C. Zhang, D. Hong, J. Li, Q. Cheng, Z. Li and W. Cai, *J. Mater. Chem.*, 2012, **22**, 13674–13681.